A Physics-Inspired Distributed Energy Equation for Macroscopic Traffic Flow Models

Brian Block, *Graduate Student Member, IEEE*, and Stephanie Stockar, *Member, IEEE*

***Abstract*— This paper presents a distributed, physics-based energy equation to be used with macroscopic traffic flow models. The proposed macroscopic energy equation is derived starting from the road load equation and it is then integrated with the Aw-Rascle-Zhang model. Results are compared against the energy output of microscopic car-following models, namely the Improved Intelligent Driver Model and the Extended Intelligent Driver Model. To enable the comparison between macroscopic and microscopic model variables, kernel density estimation is used. This allows individual vehicle positions, speeds, and energy usage obtained from the ordinary differential equations to be converted to distributed quantities. The proposed macroscopic energy equation is evaluated on three different traffic scenarios: free flow, congested traffic, and mixed traffic. It is shown that the proposed energy model can calculate the energy output within ±4% in free flow traffic, ±11% in congested traffic, and ±8% in mixed traffic.**

***Index Terms*— Macroscopic traffic flow, ARZ model, energy model, model validation.**

I. Introduction

In THE United States, transportation accounts for a large portion of total energy use. In fact, roughly 27% of energy usage comes from the transportation sector [1]. Traffic congestion plays a large role in this energy usage. In the United States, up to 3.5 billion gallons of fuel are wasted yearly as a result of congestion [2]. Because of this, much effort has been made to assess the impact of traffic on both highways and urban networks through modeling and simulation [3], [4], [5], [6].

Models of traffic mainly take two forms, microscopic and macroscopic. Microscopic models describe the individual position and acceleration of vehicles, while macroscopic models describe locally aggregated quantities such as vehicle density, flow, and mean speed [7]. The mathematical equations that govern microscopic models are ordinary differential equations (ODEs), while the equations that govern macroscopic models are partial differential equations (PDEs). Traffic simulations that rely on microscopic models can become computationally intensive when simulating large networks such as cities or highways with high vehicle flow. In these scenarios, a macroscopic model becomes advantageous [8]. However, unlike microscopic models, macroscopic models currently have no physics-based description of energy usage. Hence, while energy optimization problems that utilize microscopic models are well studied, the use of macroscopic models for energy optimization has not yet been explored as there is no distributed physics-based energy equation.

One of the most common objectives in macroscopic traffic control is to track a desired density setpoint, which in turn determines the location of traffic jams. Boundary control has been used to achieve a desired density profile through regulation of on-ramp flows in [9]. Boundary control has also been used in [10], [11], [12], and [13] to achieve a desired density profile through backstepping control, reinforcement learning, and PI control, respectively. In [14] and [15], a time dependent density profile is tracked using boundary control. In addition to boundary control, variable speed limit control, an application of in-domain control, has been used to stabilize a density profile [16]. Both ramp metering and variable speed limit control were used in a model predictive control setup in [17] to maintain queue length on on-ramps and limit capacity drop in highway sections.

In addition to density setpoint control, a significant body of literature focuses on reducing total travel time. For example, in [18], a two-class traffic flow model is controlled using ramp metering to reduce total time spent on the highway, oscillations in the control variable, and on-ramp queue length. Similarly, boundary control is used in [19] to maximize outflow, as well as to reduce the time that a vehicle stays in a highway link. Model predictive control is used in [20] in order to minimize the total travel time of vehicles and to balance density in a discrete, first-order macroscopic model. In-domain control is also used to reduce travel time. A feedback-based variable speed limit control setup is used in [21], and a moving bottleneck approach is used in [22].

While the previous control objectives are well studied, energy optimization has not been as thoroughly investigated. This is due to the lack of a physics-based energy equation for macroscopic models. Currently, any macroscopic control problems that focus on energy reduction use emissions or fuel consumption in the objective function [23], [24]. However, these representations fail to capture vehicle specific characteristics, such as aerodynamic drag, rolling resistance, or forces due to changes in grade. For example, [18] relies on an average-speed emissions model, which computes the average

Manuscript received 21 August 2023; revised 13 February 2024; accepted 23 May 2024. This work was supported in part by the National Science Foundation Graduate Research Fellowship Program under Grant DGE-1343012 and in part by the NSF CAREER Award under Grant 2042354. The Associate Editor for this article was Y. Kim. *(Corresponding author: Brian Block.)*

The authors are with the Department of Mechanical and Aerospace Engineering and the Center for Automotive Research, The Ohio State University, Columbus, OH 43212 USA (e-mail: block.168@osu.edu; stockar.1@osu.edu).

Digital Object Identifier 10.1109/TITS.2024.3416735

emissions of a given pollutant based only on the average speed over a highway link. The main problem with average-speed approaches is that they do not capture the variation in emissions or fuel consumption due to changing of speed within a highway link. An alternative to average-speed models is presented in [25], where a microscopic emission and fuel consumption model is integrated with a macroscopic traffic flow model. The methodology is to transform macroscopic data into microscopic data and then use well-known microscopic fuel consumption models. Results show that the integrated approach achieves the same fuel consumption, within 3-7%, as its microscopic counterpart (microscopic traffic flow model with microscopic fuel consumption model) while computing faster. Other attempts include using a moving bottleneck to reduce energy consumption [23], [24], where a polynomial fit of fuel consumption as function of velocity averaging the fuel consumption curves of four different vehicles is used [26]. This method, however, is limited to providing fuel consumption, not energy usage, and it does not account for the physics of the vehicles or traffic flow. Energy usage is preferred because it is powertrain agnostic, unlike fuel consumption.

The model presented in this paper is different from previous attempts as it is the first physics-based energy equation for macroscopic traffic flow. Previous energy models suffer in that they either take insufficient microscopic data or use fuel consumption as the energy metric. By using fuel consumption or emissions as the metric for energy, too many uncertainties are introduced. In going from fuel to energy used, there are many efficiencies both in the engine and drivetrain that differ between vehicles that can cause the resulting energy calculation to be incorrect. The presented model aims to fix this issue by working with just energy required at the wheel of a vehicle. This new model takes into account the physics of the problem such as aerodynamic drag, rolling resistance, and forces due to changes in grade.

In the following sections, a general framework to create a distributed, physics-based energy model for macroscopic models that mimics the energy usage of microscopic models is presented. The developed energy model, the macroscopic road load equation (MRLE), is used in conjunction with a second-order macroscopic traffic flow model. Kernel density estimation (KDE) is used so that the results of the MRLE can be compared against its microscopic counterpart. The main contributions of this paper are as follows. First a novel physics-based energy equation is derived for macroscopic model. By using a physics-based approach, the influence of aspects such as aerodynamic drag and road grade, amongst other factors, can be evaluated on the energy output of traffic. Before, this kind of analysis was not possible at the macroscopic level. In addition, a comparison is made between macroscopic models and microscopic models. This comparison shows that the newly developed model can accurately describe the energy output of macroscopic traffic, something that has not previously been done. The developed model is validated against the energy output of several microscopic models, utilizing both `MATLAB` and the popular traffic simulation software `SUMO`. It is shown that the novel MRLE provides approximately the same energy output of its microscopic counterpart in three different traffic scenarios. The remainder of the paper is structured as follows. Section II summarizes the macroscopic and microscopic models considered in this paper, while Section III presents the MRLE. Section IV presents the approach for comparing microscopic and macroscopic results via KDE. The case studies and calibration of parameters are given in Section V. The comparison results are then shown and discussed in Section VI.

II. Microscopic and Macroscopic Model Descriptions

The two main forms of traffic models are microscopic and macroscopic models. Common macroscopic models used for traffic simulation include first-order models such as the Lighthill-Whitham-Richards (LWR) model and second-order models such as the Payne-Whitham (PW) and Aw-Rascle-Zhang (ARZ) models [7], [27], [28]. The first order LWR model consists of a conservation of mass equation to determine density [29]. To determine the velocity of traffic, an equilibrium velocity equation dependent on density is used. The LWR model has several deficiencies, namely that it produces infinite deceleration when a vehicle encounters a shock and that it assumes that the equilibrium velocity assumption holds, even in non-equilibrium traffic [30]. The PW model [31] was the one of the first second-order models to replace the equilibrium velocity equation in the LWR model with a momentum equation [32]. The addition of a momentum equation solved some deficiencies of the LWR model. Second-order models are desirable as they are more realistic in capturing traffic dynamics in congestion due to the models possessing a family of flow rate curves which can accurately model the different speeds of vehicles in traffic [33]. However, the PW model is not an ideal representation of traffic flow as it has been shown that future traffic conditions can be affected by what is happening behind it and negative travel speed can occur under certain cases, which is not realistic traffic behavior [34]. In light of these problems with second-order models, a more realistic second-order model, the ARZ model, was developed [28], [30].

Microscopic models describe the position and acceleration of individual vehicles and their reactions to surrounding vehicles. Car-following models, the most common type of microscopic model, describe driver behavior based off of interactions with other vehicles in all traffic scenarios, such as free traffic, stationary traffic, and car-following situations [7], [35], [36], [37], [38], [39]. The governing equations for car-following models are ODEs that describe the acceleration of individual vehicles. To be considered a *complete* car-following model the governing acceleration equation must be a decreasing function of speed as well as an increasing function of both distance to and speed of the preceding vehicle [7]. Additionally, the model must be able to keep a minimum gap between vehicles. The Intelligent Driver Model (IDM) is one of the simplest complete car-following models [7]. The IDM uses a desired speed and following distance to describe the acceleration of individual vehicles [35]. This

model gives accurate traffic behavior, except in platooning scenarios on highways. When large strings of vehicles are following each other, following vehicles cannot achieve their desired speed so the gap between vehicles grows. To this end, the Improved Intelligent Driver Model (IIDM) was developed, which addresses the faults of the IDM [7], [37]. In the IIDM, the desired gap between vehicles no longer continues to grow past the equilibrium spacing value near the vehicles' desired speed. In [40], multiple extensions of the IDM, including the IIDM, are combined into a generalized model called the Extended Intelligent Driver Model (EIDM).

For the purpose of this paper, the MRLE is integrated with one macroscopic traffic flow model, the ARZ. The selection was made due to its ability to accurately capture traffic dynamics in all traffic scenarios. And two microscopic car-following models, namely the IIDM and EIDM, are used for comparison. The IIDM is used instead of the IDM because of the deficiency in the IDM where in large strings of vehicles, the desired speed is not met. Both the ARZ model and IIDM are implemented in `MATLAB`. In addition to `MATLAB`, the well-known microscopic traffic simulation package, `SUMO`, is used for comparison [41]. `SUMO` includes many car-following models as well as other simulation and modeling tools that can be used to either build custom routes or reconstruct real world routes. `SUMO` is also useful in handling large networks of roads or large traffic simulations with many vehicles. As well, `SUMO` has an integrated communication add-on called Traffic Control Interface (TraCI) that allows information to pass from `SUMO` to other programs [42]. In this work, TraCI is used to send information between `SUMO` and `MATLAB` in order to compare simulation results. In `SUMO`, the EIDM is the selected car-following model.

A. Aw-Rascle-Zhang Model

The ARZ model [28], [43] is defined by a set of hyperbolic PDEs that describe the flow of traffic. It includes the conservation of mass, which gives the density along a length of road; and the conservation of momentum equation, which gives the dynamic velocity:

$$\begin{aligned} &\frac{\partial \rho}{\partial t}+\frac{\partial(w+\rho V_{eq})}{\partial z}=0 \\ &\frac{\partial w}{\partial t}+\frac{\partial(\frac{w^2}{\rho}+wV_{eq})}{\partial z}=\frac{\rho}{\tau}(V_{eq}-u) \end{aligned} \tag{1}$$

where ρ is the traffic density, u is the velocity field, and τ is the relaxation time. The equilibrium velocity, V_{eq}, is a function of density given by Greenshield's model

$$V_{eq}=V_{max}(1-\frac{\rho}{\rho_{max}}) \tag{2}$$

where V_{max} is the maximum velocity, and ρ_{max} is the maximum density. The difference between the actual flow and equilibrium flow, w, is given by

$$w=\rho(u-V_{eq}) \tag{3}$$

While the ARZ model can accurately describe the density of vehicles on the road and the speed at which they travel, there is no equation in the model that captures the total energy usage along the road.

B. Improved Intelligent Driver Model

The IIDM is a car-following model consisting of a set of nonlinear ODEs that describe the position and acceleration of individual vehicles [7], [37]. It is an extension of the IDM which is simply given as

$$\dot{v}=a\left[1-\left(\frac{v}{v_0}\right)^{\delta}-\left(\frac{s^*(v,\Delta v)}{s}\right)^2\right] \tag{4}$$

where

$$s^*(v,\Delta v)=s_0+\max\left(0, vT+\frac{v\Delta v}{2\sqrt{ab}}\right) \tag{5}$$

The parameter a represents the maximum acceleration of a vehicle. A vehicle will accelerate to its desired velocity v_0. The acceleration of the vehicle will decrease as it gets closer to v_0. This decrease in acceleration is governed by the parameter δ. The greater the value of δ, the later the decrease in acceleration happens [7]. When following a lead vehicle, the safety distance is s_0+vT where s_0 is the minimum safe gap and T is the time gap. The parameter b is the maximum deceleration a vehicle should experience when approaching a slower, or stopped, vehicle. As mentioned, there are some problems with this basic model such as unrealistically large decelerations when the actual gap between vehicles is smaller than the desired gap and vehicles not being able to reach their desired speed. To remedy this, the IDM was expanded to include different acceleration functions depending on a variety of cases. This improved model is the IIDM. The improved acceleration functions differentiate between speed above and below v_0 as well as when the desired gap is greater than or less than the actual gap. They are given by

$$\begin{aligned} \frac{dv}{dt}\Big|_{v\le v_0} &= \begin{cases} a(1-(\frac{s^*}{s})^2), & s^*\ge s \\ a_{free}(1-(\frac{s^*}{s})^{\frac{2a}{a_{free}}}), & s^*<s \end{cases} \\ \frac{dv}{dt}\Big|_{v>v_0} &= \begin{cases} a_{free}+a(1-(\frac{s^*}{s})^2), & s^*\ge s \\ a_{free}, & s^*<s \end{cases} \end{aligned} \tag{6}$$

The value of a_{free} is given by

$$a_{free}=\begin{cases} a(1-(\frac{v}{v_0})^{\delta}), & v\le v_0 \\ -b(1-(\frac{v_0}{v})^{\frac{a\delta}{b}}), & v>v_0 \end{cases} \tag{7}$$

The IIDM can capture the energy usage of a vehicle by first using the road load equation to calculate the forces acting on the vehicle, and then calculating the amount of energy needed to overcome these forces. Because the IIDM is able to accurately describe the energy usage of vehicles, it serves as a good comparison for the novel MRLE.

C. Extended Intelligent Driver Model

The Extended Intelligent Driver Model (EIDM) was first introduced in [40] as an implementation of IIDM in `SUMO` with an added human driving model. In this paper, the human driving aspect of EIDM is ignored. This is because individual human driving behavior is not modeled in the ARZ model,

so for an accurate comparison it is taken out of the model. The EIDM differs from the IIDM as instead of differentiating between the cases of $v \geq v_0$ and $v < v_0$, it linearizes the changes in desired velocity. The equation for a_{free} then becomes

$$a_{free} = a(1 - (\frac{v}{v_0})^{\delta}) \tag{8}$$

and the acceleration in the EIDM is given as

$$a_{free} = \begin{cases} a(1 - (\frac{s^*}{s})^2), & s^* \geq s \\ a_{free}(1 - (\frac{s^*}{s})^{\frac{2a}{|a_{free}|}}) & s^* < s \end{cases} \tag{9}$$

It is noted that the acceleration equation (9) in the EIDM is similar to (6) when $v \leq v_0$, with the exception of using the absolute value of a_{free} in (9). This is done because a negative exponent in (9) would cause the acceleration to be unsteady at v_0 [40]. The EIDM also has other equations that limit jerk and effect drive off behavior, but those are not included in this analysis since the purpose of using the EIDM is to replicate the IIDM in SUMO.

III. Distributed Energy Equation

In microscopic models, the road load equation is often used to calculate the power, and thus energy, required for a vehicle to move [44]. In general, the road load of a vehicle can be broken down into: aerodynamic drag, road grade, inertial load, and rolling resistance from the tires. All of these quantities are specific to the individual vehicle being modeled and are a function of its speed and acceleration. In macroscopic traffic flow models, individual vehicle speed is not defined, but the flow speed is measured instead. In order to capture the energy usage of a stretch of road using a macroscopic model, the values in the road load equation need to be expanded to use the distributed values obtained from a macroscopic model, namely $u(z,t)$ and $a(z,t)$. The forces acting on the flow of traffic as a whole are given as

$$F_a = \frac{1}{2}\rho_a A_f C_d u(z,t)^2 \tag{10}$$

$$F_r = MgC_r \cos\theta \tag{11}$$

$$F_{gr} = Mg \sin\theta \tag{12}$$

$$F_m = M_{eff} a(z,t) \tag{13}$$

where ρ_a is the air density, A_f is the frontal area of the vehicle, C_d is the drag coefficient, M is the mass of the vehicle, C_r is the rolling resistance, and M_{eff} is the effective mass of the vehicle. Without loss of generality, all vehicle specific parameters are assumed to be uniform across a length of road. When considering singular vehicles, C_d is a function of intervehicle spacing. Hence, for a real world scenario, in the distributed case, C_d would be a function of density, which is a function of space. By assuming uniformity in the vehicles, in this paper C_d is constant across the entire length of road. The energy used at time t at position z can be calculated as

$$E(z,t) = \int_0^t F_a u + F_r u + F_{gr} u + F_m u \, d\tau \tag{14}$$

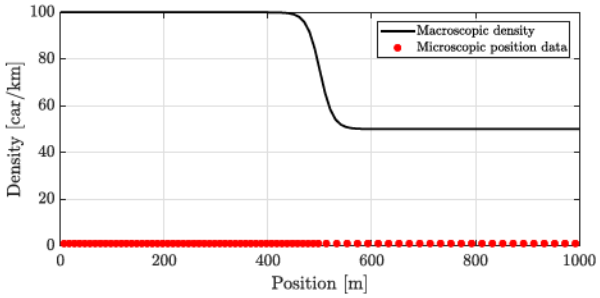

Fig. 1. Example of macroscopic conversion using KDE.

and the total energy used over the entire stretch of road at time t is given as

$$E_{total}(t) = \int_0^L E(z,t) dz \tag{15}$$

where L is the length of road.

IV. Kernel Density Estimation For Microscopic Models

To compare the results of the macroscopic and microscopic models, individual vehicle positions have to be transformed into an estimated density. This is done via Kernel Density Estimation [45]. To obtain vehicle density from individual vehicle positions, KDE is applied as follows

$$\tilde{\rho}(z,t) = \sum_{k=1}^{K} G(z - z_k(t)) \tag{16}$$

where $\tilde{\rho}(z,t)$ is the estimated density from the microscopic data at time t, K is the total number of vehicles, k is the number of an individual vehicle, G is the kernel used, z is the spatial discretization, and $z_k(t)$ is the position of vehicle k at time t. An example of this microscopic to macroscopic conversion is shown in Fig. 1. Here, the integral of $\tilde{\rho}(z,t)$ in space is equal to the total number of vehicles K. The kernel is chosen to be a Gaussian function

$$G = \frac{e^{-\frac{\chi^2}{2h^2}}}{\sqrt{2\pi}h}, \quad \chi = z - z_k(t) \tag{17}$$

where h is the is the width of the kernel, which is a parameter that must be tuned. An example of how different values of h affect the estimated density is shown in Fig. 2. If the value of h is smaller than the intervehicle spacing, then there will be unwanted peaks in the estimated density. If the value of h is too large, the reconstructed density will be affected by the boundary data and tend towards a bell curve. In the case shown in Fig. 2, $h = 10$ gives the best result as the vehicles are spaced in 10 m intervals. When intervehicle spacing is not uniform across a length of road, it becomes more difficult to tune the value of h.

Other values, such as velocity, acceleration, and energy can be found using KDE as well (16). For these values, interpolation can be used as follows

$$\tilde{\xi}(z,t) = \frac{\sum_{k=1}^{K} G(z - z_k(t))\xi_k(t)}{\| \sum_{k=1}^{K} G(z - z_k(t)) \|} \tag{18}$$

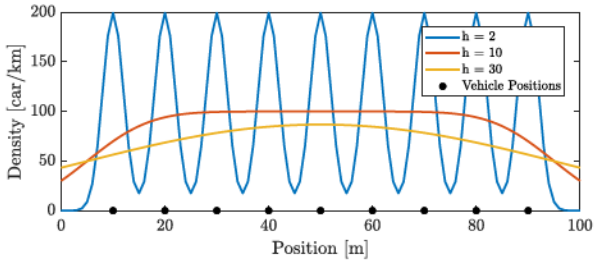

Fig. 2. Effect of h on density estimation.

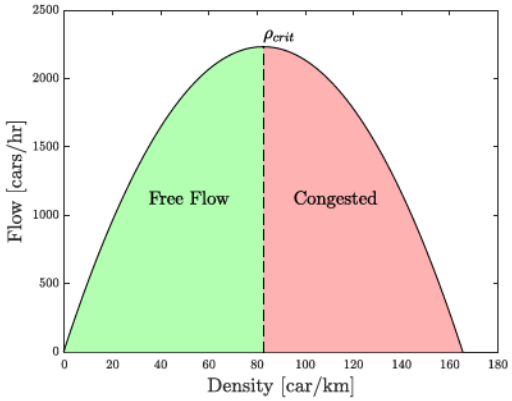

Fig. 3. Fundamental diagram showing free flow region (green) and congested region (red).

where

$$\xi = \begin{bmatrix} v_k(t) & a_k(t) & e_k(t) \end{bmatrix}^T \tag{19}$$

are the velocity, acceleration, and energy of vehicle k at time t from the microscopic models and

$$\tilde{\xi}(z,t) = \begin{bmatrix} \tilde{v}(z,t) & \tilde{a}(z,t) & \tilde{e}(z,t) \end{bmatrix}^T \tag{20}$$

are the estimated, distributed values of velocity, acceleration, and energy after KDE.

V. Simulation Case Studies and Model Calibration

A. Scenario

Three different traffic conditions are simulated to test the accuracy of the proposed MRLE. First, a free flow traffic scenario is simulated, then congested, and finally a mixed traffic case is studied. These regimes are based on the fundamental diagram shown in Fig. 3. For initial density conditions that start below the critical density, shown as ρ_{crit} in Fig. 3, we say that the traffic starts in free flow. If the traffic starts at a density that is above the critical density for the entire stretch of road, we say that it is congested. For any length of road that has a density in both the free flow and congested regimes, we say that it is a mixed traffic condition. The way traffic flow evolves in each of these scenarios is different, so it is paramount for the developed MRLE to be able to correctly characterize energy usage in all cases. The congested regime and mixed regime are the most important as that is where more energy is wasted due to traffic jams and slow moving vehicles.

For all scenarios a 1000 m long road section is simulated. All vehicles start from rest, and the inflow of vehicles is constant. The road is single lane with no on/off ramps, and there is no restriction put on the outflow of vehicles. The three initial conditions for the ARZ model are given as

$$\rho_{free}(z,0) = \frac{1}{2}\left(75 + 25 \cdot \tanh\left(\frac{-x+500}{60}\right)\right) \tag{21}$$

$$\rho_{cong}(z,0) = \frac{5}{3}\left(75 + 25 \cdot \tanh\left(\frac{-x+500}{60}\right)\right) \tag{22}$$

$$\rho_{mixed}(z,0) = 75 + 25 \cdot \tanh\left(\frac{-x+500}{60}\right) \tag{23}$$

and the boundary conditions are

$$\rho_{free}(0,t) = 50 \tag{24}$$

$$\rho_{cong}(0,t) = 165 \tag{25}$$

$$\rho_{mixed}(0,t) = 100 \tag{26}$$

These initial conditions are chosen such that the density for the entire simulation falls within the region of interest. For the free flow traffic, according to Fig. 3, traffic must stay below the critical density, which is 82.5 cars/km. For completely congested traffic, the density stays above the critical density. In the mixed case, there is both free flow and congested traffic so the initial condition must span both regions. The initial positions of the vehicles in the two microscopic models are set such that they match the initial density profiles in (21)-(23). For the microscopic models, to match the boundary conditions in (24)-(26), additional vehicles need to be simulated before the stretch of road. This technique is similar to using ghost cells in finite volume methods [46]. Both the ARZ model with the MRLE and the IIDM are simulated in `MATLAB` while the EIDM is simulated using `SUMO`.

B. Model Calibration

The parameters for the microscopic models are chosen such that the error between the microscopic and macroscopic models is minimized. Here, the error is calculated as the root mean square error (RMSE) between the velocities of the models given as

$$RMSE = \sqrt{\frac{\sum_{i=1}^{n_x \cdot n_t} (u(z,t) - \tilde{v}(z,t))^2}{n_x \cdot n_t}} \tag{27}$$

where $u(z,t)$ is the velocity field from the ARZ model and $\tilde{v}(z,t)$ is the estimated velocity field of the microscopic models obtained through KDE. The upper and lower bounds, p_{max} and p_{min}, for the parameters in (6)-(9) are given in Table I. The minimization problem is solved using `fmincon` in `MATLAB`. The ARZ model parameters are given in Table II, while the parameters for the IIDM and EIDM are calibrated based off of the ARZ parameters and are shown in Table III for each scenario. The maximum speed is taken as the nominal speed limit on a single lane road, while the maximum density is found by allowing a minimum distance between stopped vehicles of 2 m. The width of the kernel, h, is also determined via the same minimization problem, with its bounds being given in Table I. For all three case studies the width of the kernel is 49.89.

TABLE I
BOUNDS FOR MODEL PARAMETER CALIBRATION

Parameter	Unit	p_{min}	p_{max}
Desired Velocity	[m/s]	10	25
Maximum Acceleration	[m/s^2]	0.01	10
Acceleration Exponent	[-]	0.01	10
Minimum Following Distance	[m]	0.01	10
Desired Time Headway	[s]	0.01	10
Maximum Deceleration	[m/s^2]	0.01	10
Kernel Width	[-]	9	50

TABLE II
PARAMETERS FOR ARZ MODEL

Parameter	Value	Unit
V_{max}	15	[m/s]
ρ_{max}	165	[cars/km]
τ	10	[s]

TABLE III
PARAMETERS FOR IIDM AND EIDM

Parameter	Free Flow	Congested	Mixed	Units
v_0	12.21	7.95	10.01	[m/s]
a	1.20	4.98	1.30	[m/s^2]
δ	1.22	0.08	0.80	[-]
s_0	5.49	0.87	3.61	[m]
T	0.93	0.51	0.23	[s]
b	5.02	5.01	5.01	[m/s^2]

VI. RESULTS

The 1000 m long stretch of road is simulated for 45 s and the energy profile from each model is evaluated over the three different case studies. The results are evaluated based on RMSE, minimum and maximum percentage error, and mean average error (MAE). The RMSE is calculated for density and energy the same as it is in (27). The equation for MAE is given as

$$MAE = \frac{1}{n_x \cdot n_t} \sum_{i=1}^{n_x} \sum_{j=1}^{n_t} |y(z,t) - \tilde{y}(z,t)| \tag{28}$$

where $y(z,t)$ represents data from the macroscopic model and $\tilde{y}(z,t)$ represents data from the microscopic models.

A. Free Flow Traffic

The density for the free flow simulations is shown in Fig. 4 across the entire stretch of road. The results from the ARZ model are shown in Fig. 4(a), the results for IIDM are shown in Fig. 4(b), and the results using SUMO are shown in Fig. 4(c). There is good agreement between the density from the ARZ model and the estimated density from both microscopic models. The only difference in the density evolution of the different models is the density gradient after 30 s. In Fig. 4(a) and Fig. 4(b) there is an even distribution as density goes from 50 cars/km to 25 cars/km. But, in Fig. 4(c), the high density region has a slightly different shape. The resulting higher density region thus extends a little further in the EIDM simulation than in the ARZ simulation. The RMSE between the macroscopic model and microscopic models is 0.79 cars/km for both as seen in Table IV and Table V. This means that, on average, over the whole stretch of road there is only a difference of less than one car between the models. The mean average error between the models is less than 0.5 cars/km.

The resulting energy output of each model is shown in Fig. 5. The MRLE is able to capture the energy usage in a free flow traffic scenario with a maximum error of less than 1% and a minimum error of around -4%. Also, the MAE is less than 3 kJ, which shows good agreement between the models. This is good because it shows that, in the absence of traffic jams, the MRLE can accurately predict the energy usage of traffic. Now it is necessary to show that the MRLE can accurately estimate energy usage in the presence of traffic jams.

B. Congested Traffic

Congested traffic is important to model, especially when considering energy-based control, because this condition is a significant source of inefficient operation and idle time. The resulting density profiles from the congested traffic case study are shown in Fig. 6 for the ARZ model, IIDM, and SUMO. Because the traffic in the first half of the road starts at the maximum density, the vehicles in the beginning of the road are at standstill, hence zero speed. As the simulation progresses, the location of the front of the traffic jam, originally at x = 500 m, moves backwards until no part of the road is at the maximum density. The density gradient over the traffic jam is much steeper in the two microscopic models compared with the ARZ model. In the ARZ model, Fig. 6(a), no part of the road is at maximum density at around 35 s and there is a much smoother transition from higher density to lower density, as seen by the wide bands of orange, yellow, and light blue. For both the IIDM and EIDM, Fig. 6(b)-(c), the backwards propagating wave travels slower, resulting in a delayed response. In the SUMO simulation, Fig. 6(c), the first 100 m of road are still at maximum density at the end of the simulation. The steepness of the density gradient at the traffic jam location can easily be seen in Fig. 6(c), where the bands are very thin going from red to blue.

This slight mismatch in density evolution arises from the calibration of model parameters. The parameters were calibrated such that the velocity profile of the models matched, not density, so some mismatch in density is expected. This is because the desired distance between vehicles at a certain speed is different in each model, so the resulting density will be slightly different too. As well, the mismatch between the IIDM and SUMO comes from the slight differences in the acceleration function, as mentioned in Section II. Despite this difference in response time, the maximum error between the ARZ model density and IIDM density is less than 8% while the maximum error between the EIDM and ARZ model is around 11%. This difference in density results in an RMSE of 3.92 cars/km and 5.76 cars/km for the comparison between the ARZ model and IIDM and EIDM, respectively. This means that, on average, there is only about four more cars on the road in the IIDM and six more cars in the EIDM as compared to the ARZ model. The MAE between the ARZ model and IIDM

TABLE IV
ERROR BETWEEN ARZ MODEL AND IIDM FOR ALL SCENARIOS

Scenario	Density [cars/km]				Energy [kJ]			
	Max Error [%]	Min Error [%]	RMSE	MAE	Max Error [%]	Min Error [%]	RMSE	MAE
Free Flow	4.76	-4.49	0.78	0.36	0.68	-4.04	4.44	2.88
Congested	7.74	-3.99	3.92	2.39	4.04	-10.70	4.82	3.59
Mixed	6.95	-5.54	2.29	1.33	2.23	-7.48	6.56	4.97

TABLE V
ERROR BETWEEN ARZ MODEL AND EIDM FOR ALL SCENARIOS

Scenario	Density [cars/km]				Energy [kJ]			
	Max Error [%]	Min Error [%]	RMSE	MAE	Max Error [%]	Min Error [%]	RMSE	MAE
Free Flow	7.26	-5.89	0.78	0.43	0.85	-3.98	3.77	2.49
Congested	11.09	-9.32	5.76	3.53	1.03	-10.82	5.43	3.99
Mixed	5.00	-7.75	1.84	1.06	6.00	-6.61	5.88	4.66

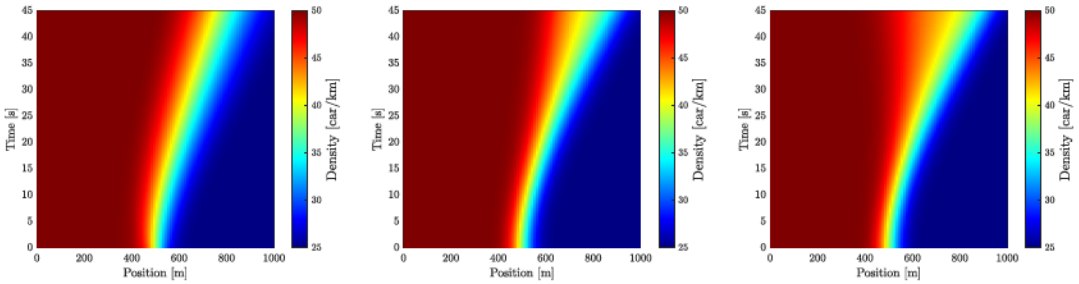

Fig. 4. Density profiles for ARZ model (a), IIDM (b), and EIDM (c) under free flow conditions.

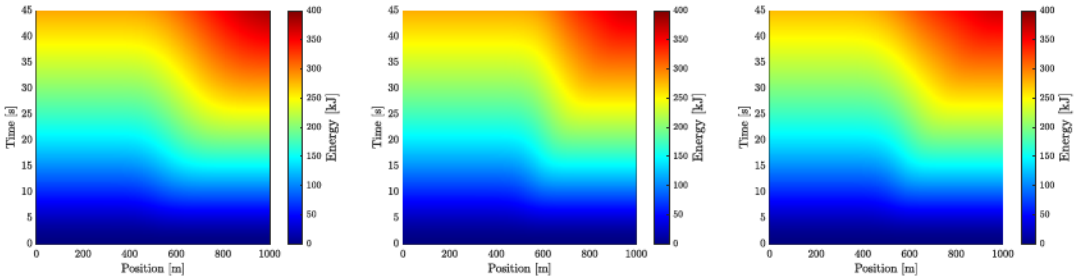

Fig. 5. Energy profiles for ARZ model (a), IIDM (b), and EIDM (c) under free flow conditions.

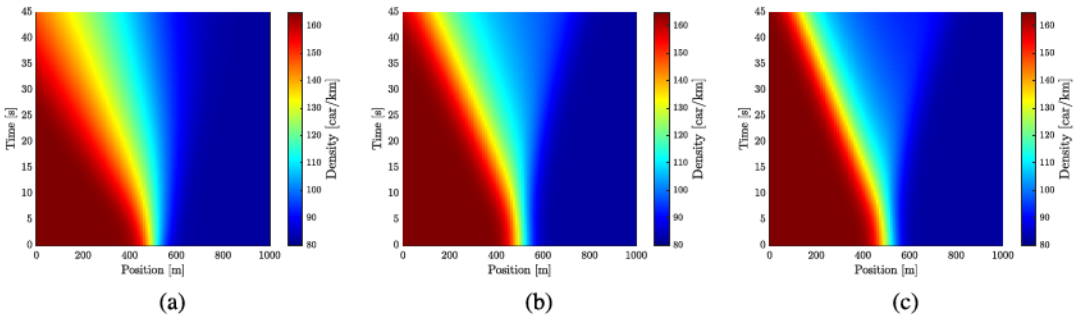

Fig. 6. Density profiles for ARZ model (a), IIDM (b), and EIDM (c) under congested conditions.

is 2.39 cars/km and between the ARZ model and EIDM it is 3.53 cars/km.

The energy profiles for all the three models are shown in Fig. 7. Overall, the MRLE matches well the energy outputs of the two microscopic models in both values and shape of the energy curves. While the shape of the curves are similar, there some small differences in the energy output. The MRLE results, shown in Fig. 7(a), have a larger region of higher

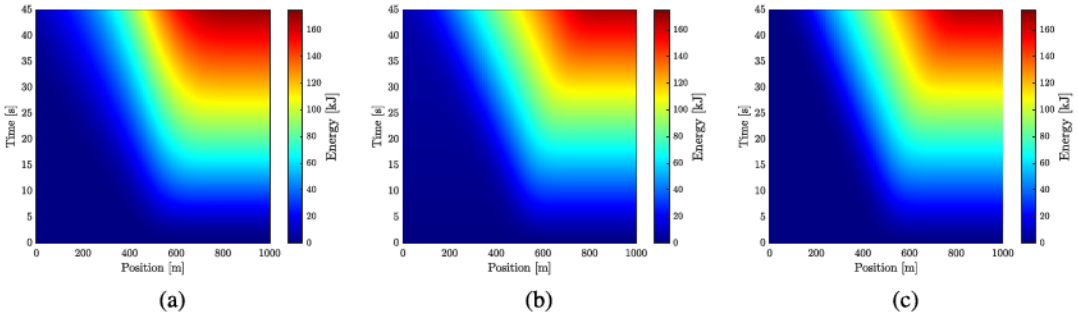

Fig. 7. Energy profiles for ARZ model (a), IIDM (b), and EIDM (c) under congested conditions.

energy usage, which is the red color on the plot. Compared with the two microscopic models, the higher energy region extends to around x = 450 m when using the MRLE and only reaches around x = 550 m at the end of the simulation for the two microscopic models. This is the result of the difference in the density curves talked about previously. The gradient between lower energy production (blue) and higher energy (red) is the same for both the MRLE and microscopic models. Overall, the MRLE over-predicts the energy usage and has an RMSE of 4.82 kJ and 5.43 kJ for the comparison with the IIDM and with the EIDM, respectively. But, this is relatively small when compared with the maximum energy usage, which is around 165 kJ. The absolute maximum energy error of the MRLE is less than 11% in comparison with both microscopic models, with most of this error coming from the difference in density gradient over the traffic jam, as mentioned before.

C. Mixed Traffic

The mixed case is the most important comparison because often times traffic will fall within both the free flow and congested regimes along a stretch of road. The comparison between density profiles for all three models is shown in Fig. 8. Since traffic falls in both the congested and free flow regime the traffic density waves in Fig. 8 fan out in both directions. Qualitatively the profiles look similar, though the propagation of the higher density front is slightly different. In both the IIDM and EIDM, the density front remains relatively the same for the first 10 s before starting to fan out. In the ARZ model, on the other hand, the density front starts to fan out immediately in an almost linear fashion. This is because the ARZ model reacts slightly quicker to changes in density than the two microscopic models. This same behavior was seen in the congested case, too, where the location of the traffic jam moved backwards along the road quicker for the ARZ model compared to the other two models. The location of the traffic jam front in the IIDM, Fig. 8(b), stays relatively constant, whereas in both the macroscopic model, Fig. 8(a), and microscopic SUMO, Fig. 8(c), simulation it starts to propagate backwards along the road. This can be seen in the lighter red section in Fig. 8(a), which is much wider than in either Fig. 8(b) or Fig. 8(c).

Finally, the energy profile obtained using the MRLE together with the ARZ model is shown in Fig. 9(a), while Fig. 9(b)-(c) shows the energy profiles of the IIDM and EIDM. There is good agreement between the results from the MRLE and from the microscopic models as the shape of the energy curves are very similar. One thing to note is that for the ARZ model and IIDM, the area from 0 - 400 m after 30 s has a slightly different shape than the SUMO simulation. The results from the ARZ model using the MRLE and IIDM give a relatively flat energy curve in this region, meaning there's no change in energy along that stretch. But, the SUMO simulation using the EIDM still has a change in energy. As mentioned before, this is because of the differences in the acceleration function using in the SUMO model. The high energy region in Fig. 9(a) also has a slightly different shape than that of Fig. 9(b) and 9(c). The energy output of the MRLE is slightly higher and this results in a steeper gradient in the section of 800 - 1000 m.

The maximum and minimum point to point error in density and energy along with the respective RMSE between the ARZ model and IIDM are shown in the last row of Table IV, while the errors between the EIDM and ARZ model are shown in the last row of Table V. The maximum and minimum errors between the ARZ model and IIDM in density fall below ±7% and below ±8% for the comparison between the ARZ model and the EIDM. Most of the error occurs after 15 s where the density in the EIDM starts to fan out more than in the ARZ model, as shown previously in Fig. 8. The RMSE in density is 2.29 cars/km for the comparison with the IIDM and only 1.84 cars/km for the comparison with the EIDM. These error values fall between the values for the free flow and congested case which is expected since the mixed case is a combination of the two previous cases. Overall, this shows very good agreement as, on average, there is only a difference of around two cars over the entire simulation domain.

In terms of energy, the MRLE is able to correctly estimate the energy usage in the mixed scenario with an absolute value maximum point to point error with the IIDM of only 7.5%. The MRLE matches the EIDM, and thus SUMO, better with an absolute maximum error of only 6.6%. Most of the error in energy between the macroscopic model and microscopic models is negative meaning that the MRLE overestimates the energy usage. This is likely due to the fact that vehicles accelerate more aggressively when starting from standstill in the macroscopic model than in either of the microscopic models. For the mixed case, the RMSE between the energy calculated using the MRLE and the microspopic models is 6.56 kJ and 5.88 kJ, respectively for the IIDM and EIDM.

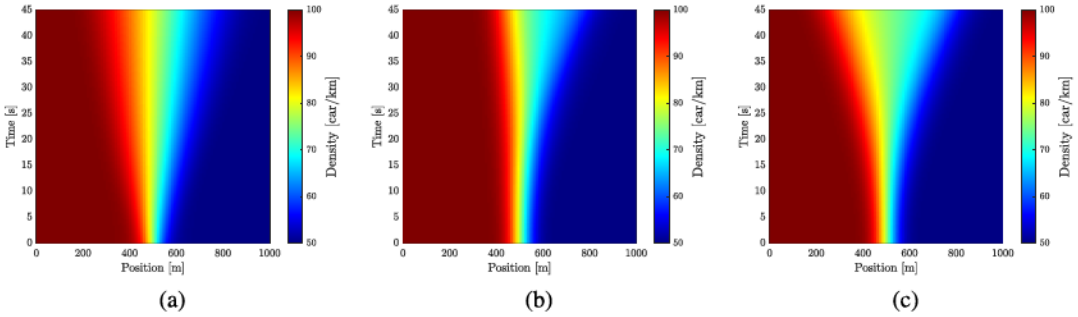

Fig. 8. Density profiles for ARZ model (a), IIDM (b), and EIDM (c) under mixed conditions.

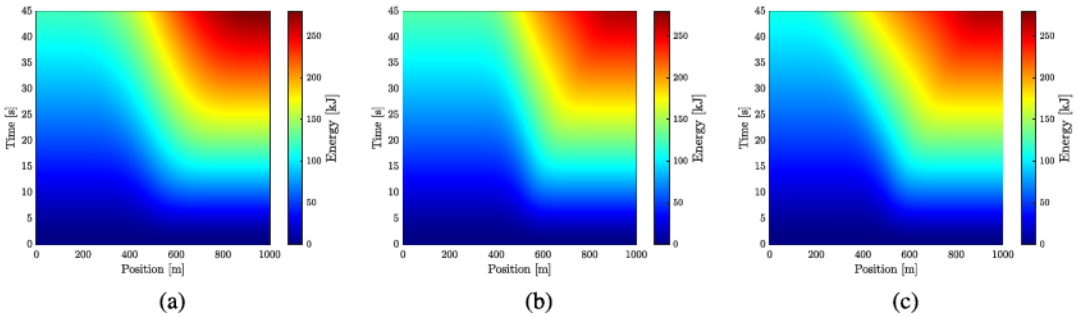

Fig. 9. Energy profiles for ARZ model (a), IIDM (b), and EIDM (c) under mixed conditions.

VII. Conclusion

This paper presented a novel physics-based, distributed energy equation for macroscopic models. First, one macroscopic traffic flow model, the ARZ model, and two microscopic car-following models, the IIDM and EIDM, were presented. Then, kernel density estimation was used to convert the individual vehicle trajectories to their macroscopic counterparts so that the ARZ model with the distributed energy equation could be compared to the microscopic results. Then a case study was presented and the parameters of the microscopic models were calibrated such that their velocity profiles matched that of the ARZ model. The proposed MRLE was then evaluated in different traffic scenarios to test its accuracy. It was shown that, in most cases, the MRLE was capable of producing the same results as SUMO as well as another microscopic traffic model, within $\pm 10\%$. Both the macroscopic ARZ model and microscopic IIDM and EIDM reproduce accurate traffic results and the developed MRLE is similar to the energy equations used for microscopic models. Because of this, the developed model has a low error in all scenarios when compared against microscopic models. These results are particularly promising in light of energy minimization problems for large scale traffic simulation. A shortcoming of this study is that the influence of road grade and drag coefficient were not investigated. On a real road, the change in grade would be enough to affect the energy usage of the vehicles traveling over it. In this study, that influence was ignored. In future work, that will be considered to better characterize energy usage. As well, the drag coefficient is currently modeled as a constant, but should be modeled as a function of density. This is left for future work.

One of the future challenges is combining this work with current traffic control literature to setup energy minimization problems. Currently, energy minimization problems are common in individual vehicles, but when the problem gets too large, or there are too many vehicles to model, real time computation of the control problem may not be possible. So, it becomes advantageous to use a macroscopic traffic PDE model for control. The issues lie in how to set up the minimization problem and how to control the traffic flow. Currently work is being done to define a control method that is able to handle both energy minimization and other control objectives such as maximizing traffic outflow, tracking a desired density profile, and reducing time spent in traffic jams.

References

[1] U.S. Energy Information Administration. (Oct. 2023). *Monthly Energy Review*. [Online]. Available: https://www.eia.gov/totalenergy/data/monthly/

[2] D. Schrank, T. Lomax, and B. Eisele. (2021). *2021 Urban Mobility Report*. Texas Transp. Inst. [Online]. Available: http://mobility.tamu.edu/ums/report

[3] A. Spiliopoulou, M. Kontorinaki, M. Papageorgiou, and P. Kopelias, "Macroscopic traffic flow model validation at congested freeway off-ramp areas," *Transp. Res. C, Emerg. Technol.*, vol. 41, pp. 18–29, Apr. 2014.

[4] F. Belletti, M. Huo, X. Litrico, and A. M. Bayen, "Prediction of traffic convective instability with spectral analysis of the Aw–Rascle–Zhang model," *Phys. Lett. A*, vol. 379, no. 38, pp. 2319–2330, Oct. 2015.

[5] M. Burger, S. Göttlich, and T. Jung, "Derivation of second order traffic flow models with time delays," *Netw. Heterogeneous Media*, vol. 14, no. 2, pp. 265–288, 2019.

[6] B. Block, X. Chen, and S. Stockar, "Stabilization of a POD/Galerkin reduced order payne-whitham traffic model *," in *Proc. Amer. Control Conf. (ACC)*, May 2023, pp. 4443–4448.

[7] M. Treiber and A. Kesting, *Traffic Flow Dynamics: Data, Models and Simulation*. Cham, Switzerland: Springer, 2012.

[8] A. Kotsialos and M. Papageorgiou, "The importance of traffic flow modeling for motorway traffic control," *Netw. Spatial Econ.*, vol. 1, pp. 179–203, Jan. 2001.

[9] C. Pasquale, S. Sacone, and S. Siri, "Closed-loop stability of freeway traffic systems with ramp metering control," in *Proc. IEEE Conf. Decis. Control (CDC)*, Dec. 2018, pp. 223–228.

[10] H. Yu and M. Krstic, "Traffic congestion control for Aw–Rascle–Zhang model," *Automatica*, vol. 100, pp. 38–51, Feb. 2019.

[11] H. Yu, S. Park, A. Bayen, S. Moura, and M. Krstic, "Reinforcement learning versus PDE backstepping and PI control for congested freeway traffic," 2019, *arXiv:1904.12957*.

[12] L. Zhang, C. Prieur, and J. Qiao, "PI boundary control of linear hyperbolic balance laws with stabilization of ARZ traffic flow models," *Syst. Control Lett.*, vol. 123, pp. 85–91, Jan. 2019.

[13] I. Karafyllis, N. Bekiaris-Liberis, and M. Papageorgiou, "Analysis and control of a non-standard hyperbolic PDE traffic flow model," 2017, *arXiv:1707.02209*.

[14] L. Tumash, C. Canudas-de-Wit, and M. L. D. Monache, "Boundary control design for traffic with nonlinear dynamics," *IEEE Trans. Autom. Control*, vol. 67, no. 3, pp. 1301–1313, Mar. 2022.

[15] L. Tumash, C. Canudas-de-Wit, and M. L. Delle Monache, "Robust tracking control design for fluid traffic dynamics," in *Proc. IEEE 58th Conf. Decis. Control (CDC)*, Dec. 2019, pp. 4085–4090.

[16] I. Karafyllis and M. Papageorgiou, "Feedback control of scalar conservation laws with application to density control in freeways by means of variable speed limits," *Automatica*, vol. 105, pp. 228–236, Jul. 2019.

[17] A. Muralidharan and R. Horowitz, "Computationally efficient model predictive control of freeway networks," *Transp. Res. C, Emerg. Technol.*, vol. 58, pp. 532–553, Sep. 2015.

[18] C. Pasquale, D. Anghinolfi, S. Sacone, S. Siri, and M. Papageorgiou, "A comparative analysis of solution algorithms for nonlinear freeway traffic control problems," in *Proc. IEEE 19th Int. Conf. Intell. Transp. Syst. (ITSC)*, Nov. 2016, pp. 1773–1778.

[19] H. Liu, C. Claudel, and R. B. Machemehl, "A stochastic formulation of the optimal boundary control problem involving the lighthill whitham Richards model," *IFAC-PapersOnLine*, vol. 51, no. 9, pp. 337–342, 2018.

[20] D. Pisarski and C. Canudas-de-Wit, "Nash game-based distributed control design for balancing traffic density over freeway networks," *IEEE Trans. Control Netw. Syst.*, vol. 3, no. 2, pp. 149–161, Jun. 2016.

[21] R. C. Carlson, I. Papamichail, and M. Papageorgiou, "Local feedback-based mainstream traffic flow control on motorways using variable speed limits," *IEEE Trans. Intell. Transp. Syst.*, vol. 12, no. 4, pp. 1261–1276, Dec. 2011.

[22] M. Čičić and K. H. Johansson, "Traffic regulation via individually controlled automated vehicles: A cell transmission model approach," in *Proc. 21st Int. Conf. Intell. Transp. Syst. (ITSC)*, Nov. 2018, pp. 766–771.

[23] G. Piacentini, P. Goatin, and A. Ferrara, "Traffic control via moving bottleneck of coordinated vehicles," *IFAC-PapersOnLine*, vol. 51, no. 9, pp. 13–18, 2018.

[24] T. Liard, R. Stern, and M. L. Delle Monache, "Optimal driving strategies for traffic control with autonomous vehicles," *IFAC-PapersOnLine*, vol. 53, no. 2, pp. 5322–5329, 2020.

[25] S. K. Zegeye, B. De Schutter, J. Hellendoorn, E. A. Breunesse, and A. Hegyi, "Integrated macroscopic traffic flow, emission, and fuel consumption model for control purposes," *Transp. Res. C, Emerg. Technol.*, vol. 31, pp. 158–171, Jun. 2013.

[26] R. A. Ramadan and B. Seibold, "Traffic flow control and fuel consumption reduction via moving bottlenecks," 2017, *arXiv:1702.07995*.

[27] V. Knoop, *Introduction to Traffic Flow Theory: An Introduction With Exercises*. Delft, The Netherlands: TU Delft Open, 2017.

[28] A. Aw and M. Rascle, "Resurrection of 'second order' models of traffic flow," *SIAM J. Appl. Math.*, vol. 60, no. 3, pp. 916–938, Jan. 2000.

[29] M. J. Lighthill and G. B. Whitham, "On kinematic waves II. A theory of traffic flow on long crowded roads," *Proc. Roy. Soc. London. A Math. Phys. Sci.*, vol. 229, no. 1178, pp. 317–345, 1955.

[30] H. M. Zhang, "A theory of nonequilibrium traffic flow," *Transp. Res. B, Methodol.*, vol. 32, no. 7, pp. 485–498, Sep. 1998.

[31] H. J. Payne, "Model of freeway traffic and control," *Math. Model Public Syst.*, vol. 1, pp. 51–61, Mar. 1971.

[32] W. Jin and H. Zhang, "Solving the Payne–Whitham traffic flow model as a hyperbolic system of conservation laws with relaxation," Univ. California Davis, Davis, CA, USA, Tech. Rep. UCD-ITS-Zhang-2001-1, 2001.

[33] S. Fan, M. Herty, and B. Seibold, "Comparative model accuracy of a data-fitted generalized Aw–Rascle–Zhang model," *Netw. Heterogeneous Media*, vol. 9, no. 2, pp. 239–268, 2014.

[34] C. F. Daganzo, "Requiem for second-order fluid approximations of traffic flow," *Transp. Res. B, Methodol.*, vol. 29, no. 4, pp. 277–286, 1995.

[35] M. Treiber, A. Hennecke, and D. Helbing, "Congested traffic states in empirical observations and microscopic simulations," *Phys. Rev. E, Stat. Phys. Plasmas Fluids Relat. Interdiscip. Top.*, vol. 62, no. 2, p. 1805, 2000.

[36] S. Gupta, S. R. Deshpande, P. Tulpule, M. Canova, and G. Rizzoni, "An enhanced driver model for evaluating fuel economy on real-world routes," *IFAC-PapersOnLine*, vol. 52, no. 5, pp. 574–579, 2019.

[37] A. Kesting, M. Treiber, and D. Helbing, "Enhanced intelligent driver model to access the impact of driving strategies on traffic capacity," *Philosophical Trans. Roy. Soc. A, Math., Phys. Eng. Sci.*, vol. 368, no. 1928, pp. 4585–4605, Oct. 2010.

[38] R. M. Malinauskas, "The intelligent driver model: Analysis and application to adaptive cruise control," Ph.D. dissertation, Dept. Math., Clemson Univ., Clemson, SC, USA, 2014.

[39] A. Kesting, M. Treiber, and D. Helbing, "General lane-changing model MOBIL for car-following models," *Transp. Res. Rec., J. Transp. Res. Board*, vol. 1999, no. 1, pp. 86–94, Jan. 2007.

[40] D. Salles, S. Kaufmann, and H.-C. Reuss, "Extending the intelligent driver model in sumo and verifying the drive off trajectories with aerial measurements," in *Proc. SUMO User Conf.*, 2020, pp. 1–25.

[41] P. A. Lopez et al., "Microscopic traffic simulation using SUMO," in *Proc. 21st Int. Conf. Intell. Transp. Syst. (ITSC)*, Sep. 2018, pp. 2575–2582.

[42] A. Wegener, M. Piórkowski, M. Raya, H. Hellbrück, S. Fischer, and J.-P. Hubaux, "TraCI: An interface for coupling road traffic and network simulators," in *Proc. 11th Commun. Netw. Simulation Symp.*, 2008, pp. 155–163.

[43] A. I. Delis, I. K. Nikolos, and M. Papageorgiou, "High-resolution numerical relaxation approximations to second-order macroscopic traffic flow models," *Transp. Res. C, Emerg. Technol.*, vol. 44, pp. 318–349, Jul. 2014.

[44] T. Gillespie, *Fundamentals of Vehicle Dynamics*. Warrendale, PA, USA: SAE International, 2021.

[45] S. Mollier, M. L. D. Monache, C. Canudas-de-Wit, and B. Seibold, "Two-dimensional macroscopic model for large scale traffic networks," *Transp. Res. B, Methodol.*, vol. 122, pp. 309–326, Apr. 2019.

[46] R. J. LeVeque, *Finite Volume Methods for Hyperbolic Problems*, vol. 31. Cambridge, U.K.: Cambridge Univ. Press, 2002.

Brian Block (Graduate Student Member, IEEE) received the Bachelor of Science degree in mechanical engineering from The Pennsylvania State University, State College, PA, USA, in 2019. He is currently pursuing the Ph.D. degree with The Ohio State University, Columbus, OH, USA. His research interests include optimization and control in partial differential equations and its application to macroscopic traffic flow.

Stephanie Stockar (Member, IEEE) received the B.S. and M.S. degrees in mechanical engineering from ETH Zürich in 2007 and 2010, respectively, and the Ph.D. degree in mechanical engineering from The Ohio State University (OSU) in 2013.

She is currently an Assistant Professor with the Department of Mechanical and Aerospace Engineering, OSU. Prior to joining OSU in 2019, she was a Research Associate with the Center for Automotive Research, OSU, and an Assistant Professor of mechanical engineering with Penn State University. Her research interests include optimal control of energy systems, particularly in the context of automotive systems, mobility, and smart cities. Her interdisciplinary approach combines thermo-fluid sciences, dynamic systems, modeling, optimization, and control theory. She is a member of ASME and SAE.